Preprints.org

Article

Not peer-reviewed version

Functional and Expression Studies of iPSC-Derived Cardiomyocytes Carrying a Novel HCM-Associated MYPN Genetic Variant

Elena V. Dementyeva , Ekaterina S. Klimenko , Margarita Y. Sorokina , Anastasia K. Zaytseva , Maxim T. Ri , Ekaterina G. Nikitina , Dmitriy A. Kudlay , Anna M. Zlotina , Svetlana I. Tarnovskaya , Yuri V. Vyatkin , Dmitriy N. Shtokalo , Suren M. Zakian , Anna A. Kostareva *

Posted Date: 22 December 2025

doi: 10.20944/preprints202512.1808.v1

Keywords: myopalladin; hypertrophic cardiomyopathy; genetic variants; induced pluripotent stem cells; cardiomyocytes

Preprints.org is a free multidisciplinary platform providing preprint service that is dedicated to making early versions of research outputs permanently available and citable. Preprints posted at Preprints.org appear in Web of Science, Crossref, Google Scholar, Scilit, Europe PMC.

Copyright: This open access article is published under a Creative Commons CC BY 4.0 license, which permit the free download, distribution, and reuse, provided that the author and preprint are cited in any reuse.

Preprints.org (www.preprints.org) | NOT PEER-REVIEWED | Posted: 22 December 2025 doi:10.20944/preprints202512.1808.v1

Disclaimer/Publisher's Note: The statements, opinions, and data contained in all publications are solely those of the individual author(s) and contributor(s) and not of MDPI and/or the editor(s). MDPI and/or the editor(s) disclaim responsibility for any injury to people or property resulting from any ideas, methods, instructions, or products referred to in the content.

Article

Functional and Expression Studies of iPSC-Derived Cardiomyocytes Carrying a Novel HCM-Associated *MYPN* Genetic Variant

Elena V. Dementyeva [1,2], Ekaterina S. Klimenko [3], Margarita Y. Sorokina [3], Anastasia K. Zaytseva [3], Maxim T. Ri [4], Ekaterina G. Nikitina [3], Dmitriy A. Kudlay [5,6,7], Anna M. Zlotina [3], Svetlana I. Tarnovskaya [8], Yuri V. Vyatkin [9,10], Dmitriy N. Shtokalo [10,11], Suren M. Zakian [1,2] and Anna A. Kostareva [3,12,*]

1 Institute of Cytology and Genetics, Siberian Branch of the Russian Academy of Sciences, Novosibirsk, Russia
2 Institute of Chemical Biology and Fundamental Medicine, Siberian Branch of the Russian Academy of Sciences, Novosibirsk, Russia
3 Almazov National Medical Research Centre, Institute of Molecular Biology and Genetics, Saint-Petersburg, Russia
4 The Center for Molecular and Cellular Biology, Moscow, Russia
5 Department of Pharmacognosy and Industrial Pharmacy, Faculty of Fundamental Medicine, Lomonosov Moscow State University, Moscow, Russia
6 Department of Pharmacology at the Institute of Pharmacy, Sechenov First Moscow State Medical University (Sechenov University), Moscow, Russia
7 NRC Institute of Immunology FMBA of Russia, Moscow, Russia
8 Sechenov Institute of Evolutionary Physiology & Biochemistry, Russian Academy of Sciences, St. Petersburg, Russia
9 Novel Software Systems, Novosibirsk, Russia
10 AcademGene LLC, Novosibirsk, Russia
11 A.P. Ershov Institute of Informatics Systems, Siberian Branch of the Russian Academy of Sciences, Novosibirsk, Russia
12 Karolinska University Hospital, Karolinska Institutet, Department of Women's and Children's Health, Stockholm, Sweden
* Correspondence: akostareva@hotmail.com

Abstract

Variants in *MYPN* encoding a sarcomeric protein, myopalladin, are associated with different types of cardiomyopathies and myopathies. However, molecular mechanisms of *MYPN*-associated pathologies are still poorly understood. In this study, we generated induced pluripotent stem cells (iPSCs) from a hypertrophic cardiomyopathy patient carried a novel p.N989I (c.2966A>T) variant in *MYPN* and used iPSC-derived cardiomyocytes to examine the impact of the variant on biophysical characteristics and transcriptomic profile. No significant changes in parameters of calcium transient, sodium current and action potential were found in iPSC-derived cardiomyocytes with p.N989I (c.2966A>T) variant in *MYPN* compared to control cells from a healthy donor. At the transcriptomic level, *MYPN*-N989I cardiomyocytes demonstrated an upregulation of genes linked to cell cycle, division springle, microtubule cytoskeleton organization and myogenic program genes. A downregulation of sarcomeric, Z-disc- and cell junction-associated genes and genes involved in ATP synthesis, oxidative phosphorylation and SRF-signaling pathway was also revealed. Our data suggest that the p.N989I (c.2966A>T) variant in *MYPN* plays a dual role in hypertrophic cardiomyopathy pathogenesis, disrupting not only sarcomeric and cytoskeletal organization but also muscle gene program regulation.

Keywords: myopalladin; hypertrophic cardiomyopathy; genetic variants; induced pluripotent stem cells; cardiomyocytes

© 2025 by the author(s). Distributed under a Creative Commons CC BY license.

Preprints.org (www.preprints.org) | NOT PEER-REVIEWED | Posted: 22 December 2025 doi:10.20944/preprints202512.1808.v1

1. Introduction

Myopalladin encoded by *MYPN* gene was identified over twenty years ago as one of the key α-actinin binding proteins, which takes part in actin cytoskeleton organization, polymerization and stability [1]. Based on its homology with earlier described palladin and myotillin, myopalladin was demonstrated to have an important role in actin filament assembly of both sarcomeric and cytoskeletal pools of F-actin in muscle cells. Being a striated muscle-specific protein, it is localised in I-band and Z-line of sarcomeric structure and interacts with several structural components of Z-disc, such as nebulette and titin. Myopalladin is also capable to interact with nucleus-translocating proteins of Z-disc area, CARP and ANKRD2. The latter fact arguments for mechanostransduction function of myopalladin, making it one of the important regulators of contractility strength and relaxation through initiating several gene expression programs. The ability of myopalladin to provide a structural integrity of Z-disc [2] and to translocate to the nucleus together with CARP makes it a possible regulator of myogenic gene program through interaction with SRF and regulation of cell cycle-related genes. In addition, *MYPN*-knockout mice demonstrate the alteration in several signalling pathways and kinase expression such as mitogen-activated protein kinases Erk1/2, JNK, PAK1 as well as Akt-phosphorylation [3]. All together this confirms the important role of *MYPN* in Z-line architecture and stress-detecting signalling of striated muscle cells.

Being a Z-line associated protein of sarcomere, *MYPN* attracts attention as a possible cardiomyopathy and myopathy causative gene. Similar to other Z-line proteins, myopalladin has been described in connection to several types of cardiomyopathies – hypertrophic (HCM) [4,5], dilated (DCM) [6–8], restrictive (RCM) and left-ventricular non-compaction [9]. It was also detected as a causative gene for slow progressive congenital cap myopathy – a subtype of nemaline myopathy – with autosomal recessive inheritance [10].

Earlier we described a HCM patient carried a novel p.N989I (c.2966A>T) variant in *MYPN* [11]. The substitution is localized to the alpha-actinin-interacting region of the protein [1] and posesses the pathogenic properties according to *in silico* analysis data. However, clinical significance of the variant and possible mechanisms underlying its pathogenicity remain unknown. Generating induced pluripotent stem cells (iPSCs) from HCM patients and their subsequent differentiation into cardiomyocytes have been successfully used to create cell models for unraveling pathogenetic mechanisms of the disease [12–22]. In this study, we applied the iPSC-based approach to generate the first cell model for HCM caused by a *MYPN* variant. To decipher the role of *MYPN* and the p.N989I (c.2966A>T) variant in HCM pathogenesis, we analysed functional properties (characteristics of calcium transients, sodium currents and action potentials) and transcriptome profile of iPSC-derived cardiomyocytes.

2. Results

2.1. Structural Analysis of MYPN-N989I Variant

A new p.N989I (c.2966A>T) variant in *MYPN* was earlier described in a patient with HCM and no familial history of inherited cariac disorders [11]. Myopalladin contains five immunoglobulin-like domains. Structural modelling identified this variant to be located in the third Ig domain of myopalladin (Figure 1a). This domain is known as actinin-interacting domain and contributes for direct F-actin binding [3]. The variant resides in a highly conserved position among different species (Figure 1b). Alignment of the myopalladin Ig3 domain with homologous Ig domains shows low similarity of this position (Figure 1c). Myopalladin Ig3 is highly similar with the palladin actin-binding domain Ig3, which consists of seven antiparallel β-strands forming a barrel-like shape (Figure 1c,d) [23]. Within Ig structure, the variant fells in the loop between C and D β-strands (Figure

© 2025 by the author(s). Distributed under a Creative Commons CC BY license.

Preprints.org (www.preprints.org) | NOT PEER-REVIEWED | Posted: 22 December 2025 doi:10.20944/preprints202512.1808.v1

1d; PDB: 2LQR, chain A). Moreover, ClinPred and AlphaMissense tools predict p.N989I variant as pathogenic.

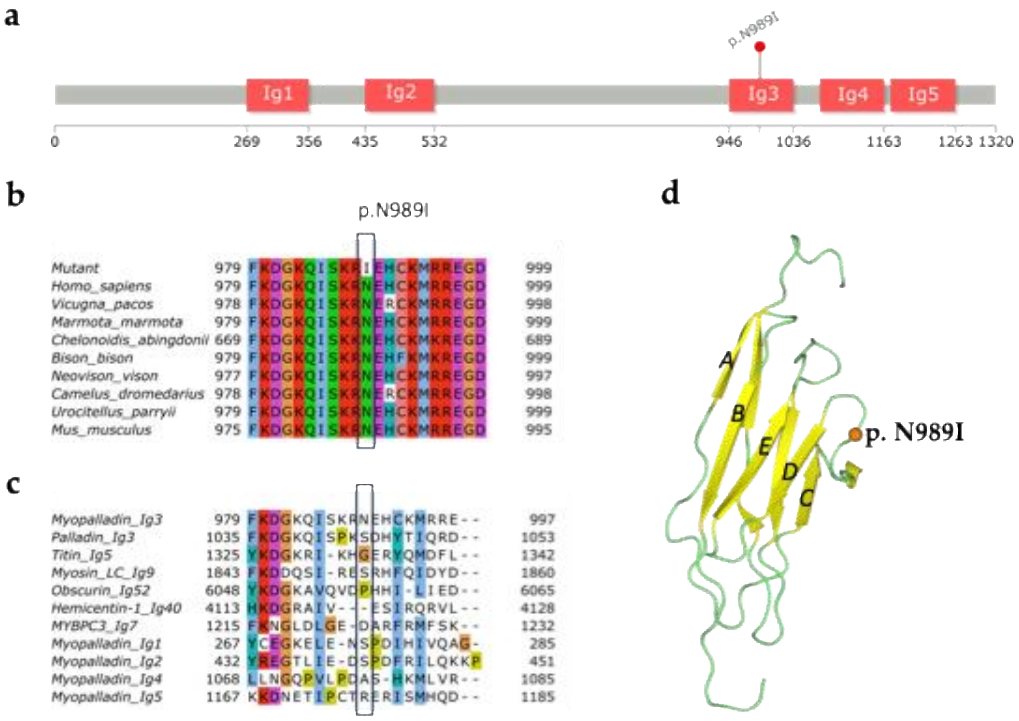

Figure 1. Localization of p.N989I variant in immunoglobulin-like domain 3 of myopalladin. (**a**) Domain organization of myopalladin (UniprotKB: Q86TC9) and localization of the p.N989I variant performed using InterPro database [24] and lollipops tool [25]. Immunoglobulin-like domains are marked as 'Ig'. p.N989I fell in Ig3 domain of myopalladin; (**b**) A multiple sequence alignment of human myopalladin with orthologues; (**c**) A multiple sequence alignment of Ig3 domain of human myopalladin with Ig-domains of homologous human proteins. p.N989I is located at a variable position within the alignment of the domains. Each residue in the alignment is colored using Clustal X Colour Scheme: blue - hydrophobic; red – positive charged; magenta – negative charged; green – polar; pink – cysteines; orange – glycines; yellow – prolines; cyan – aromatic; white – unconserved; (**d**) 3D structure of palladin Ig3 domain (PDB:2LQR) [23]. p.N989I is mapped on the structure according to the sequence alignment. Substitution fell in the linker (green) between C and D strands (yellow).

2.2. Generation of MYPN-N989I iPSC Lines and Directed Differentiation into Cardiomyocytes

Mononuclear cells (MNCs) of the patient carrying a heterozygous p.N989I (c.2966A>T) variant in *MYPN* were reprogrammed to the pluripotent state using transfection with episomal vectors expressed *OCT4*, *SOX2*, *KLF4*, *L-MYC* and *LIN28* [26]. The cell lines generated demonstrated human pluripotent stem cell-like morphology (Figure 2a) and were negative for mycoplasma presence (Figure 2b). Based on analysis of episome elimination (Figure 2c), two cell lines, FAMRCi015-A and FAMRCi015-B, were selected for further characterization. Pluripotent state of the cell lines was confirmed by expression of pluripotency markers (the *OCT4*, *NANOG*, *SOX2* genes and SSEA4, TRA-1-60 surface antigens) and capacity to give rise to derivatives of three germ layers during spontaneous differentiation in embryoid bodies (Figure 2d-f). The iPSC lines retained a normal karyotype, 46,XX, (Figure 2g) and p.N989I (c.2966A>T) variant in *MYPN* (Figure 2h). STR analysis showed that the iPSC lines were identical to the MNCs used for their generation at 26 polimorphic loci (data not shown).

© 2025 by the author(s). Distributed under a Creative Commons CC BY license.

Preprints.org (www.preprints.org) | NOT PEER-REVIEWED | Posted: 22 December 2025 doi:10.20944/preprints202512.1808.v1

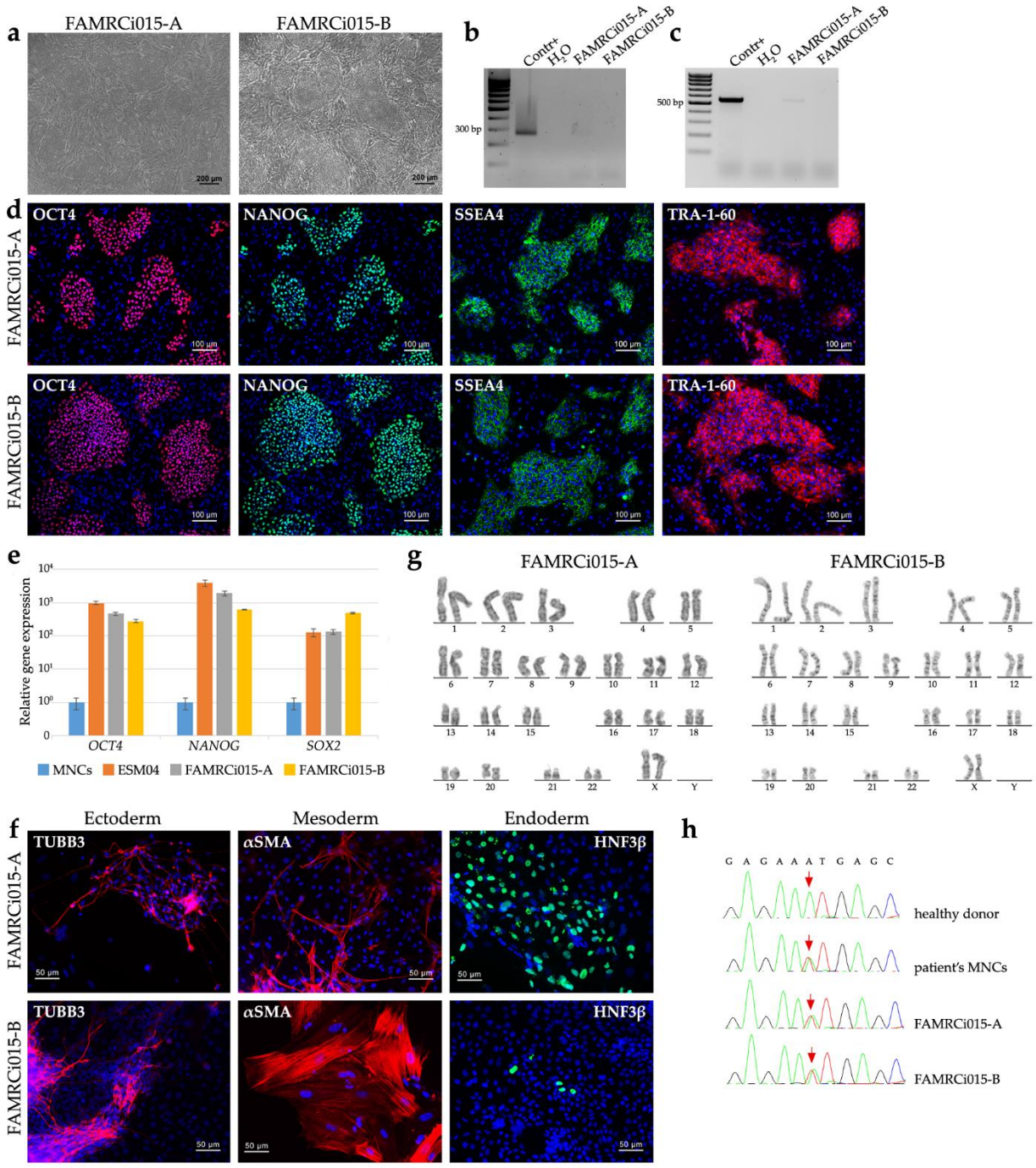

Figure 2. Characterization of iPSC lines generated by reprogramming of the mononuclear cells from the patient with p.N989I (c.2966A>T) variant in *MYPN*. (**a**) FAMRCi015-A and FAMRCi015-B iPSC lines have a morphology characteristic to human pluripotent stem cells. Scale bar – 200 µm; (**b**) Absence of mycoplasma contamination in the patient-specific iPSC lines. Contr+, positive control for mycoplasma contamination. H_2O, negative control; (**c**) Episome elimination in the FAMRCi015-A and FAMRCi015-B iPSC lines. Contr+, positive control for episome presence, an iPSC line at an early passage. H_2O, negative control; (**d**) Patient-specific iPSC lines express a number of pluripotent state markers – the OCT4 and NANOG transcription factors and SSEA4 and TRA-1-60 surface antigens. Scale bar – 100 µm; (**e**) Positive expression of pluripotency genes, *OCT4*, *NANOG* and *SOX2*, in the FAMRCi015-A and FAMRCi015-B iPSC lines. MNCs, patient's mononuclear cells. ESM04, a line of human embryonic stem cells used as a positive control of *OCT4*, *NANOG* and *SOX2* expression. Data are presented as mean ± SD; (**f**) Patient-specific iPSC lines are able to be differentiated into derivatives of three germ layers – ectoderm (TUBB3, βIII-tubulin), mesoderm (αSMA, smooth muscle alpha-actinin) and endoderm (HNF3β, hepatocyte nuclear factor 3 beta). Scale bar – 50 µm; (**g**) FAMRCi015-A and FAMRCi015-B iPSC lines have a normal karyotype – 46,XX; (**h**) iPSC lines retain the patient-specific heterozygous p.N989I (c.2966A>T)

© 2025 by the author(s). Distributed under a Creative Commons CC BY license.

Preprints.org (www.preprints.org) | NOT PEER-REVIEWED | Posted: 22 December 2025 doi:10.20944/preprints202512.1808.v1

substitution. The nucleotide sequence of a part of *MYPN* exon 14 in a healthy donor and the patient's mononuclear cells (MNCs) are given for comparison. The position where the c.2966A>T substitution occurs in the HCM patient is indicated by red arrows.

The patient-specific iPSC lines, FAMRCi015-A and FAMRCi015-B, together with a commercially available iPSC line from a healthy donor, WTSIi046-A (Sigma-Aldrich, Darmstadt, Germany, Cat # 66540120), were differentiated into cardiomyocytes. The protocol based on Wnt activation with the GSK3β protein kinase inhibitor (CHIR99021) followed by Wnt inhibition with IWR1 was used first [27]. Zones of spontaneous contractions formed on days 8-9 of differentiation. To isolate pure population of cardiomyocytes, differentiated cells were subjected from day 9 to day 15 of differentiation to metabolic selection in glucose-free medium supplemented with sodium DL-lactate [27]. Purified cardiomyocytes were cultivated for two weeks in the presence of 2μM CHIR99021 for their proliferation and for another two weeks in the medium contained low glucose and high oxidative substrate concentrations [28] to promote maturation of iPSC-derived cardiomyocytes. The fact that the cells obtained were predominantly cardiomyocytes was verified by expression of cardiac troponin I on day 48 of differentiation (Figure S1). iPSC-derived cardiomyocytes from the patient with p.N989I (c.2966A>T) variant in *MYPN* (*MYPN*-N989I-CMs) and the healthy donor (Donor-CMs) were used for functional studies and transcriptome analysis to study the impact of the p.N989I (c.2966A>T) variant in *MYPN* on cardiomyocyte structure and function.

2.3. Calcium Dynamics Is Not Altered in iPSC-Derived Cardiomyocytes with p.N989I Variant in MYPN

MyoPacer field stimulation and IonOptix setup were used to measure parameters of calcium transient in the iPSC-derived cardiomyocytes. Transient duration (time to 90% baseline), pre-peak parameters (time to peak and calcium release velocity), transient Ca^{2+} amplitude and post-peak parameters (time to baseline and calcium return velocity) did not differ significantly between *MYPN*-N989I-CMs and Donor-CMs (Figure 3). To sum up, intracellular cytosolic calcium oscillations in *MYPN*-N989I-CMs were not affected.

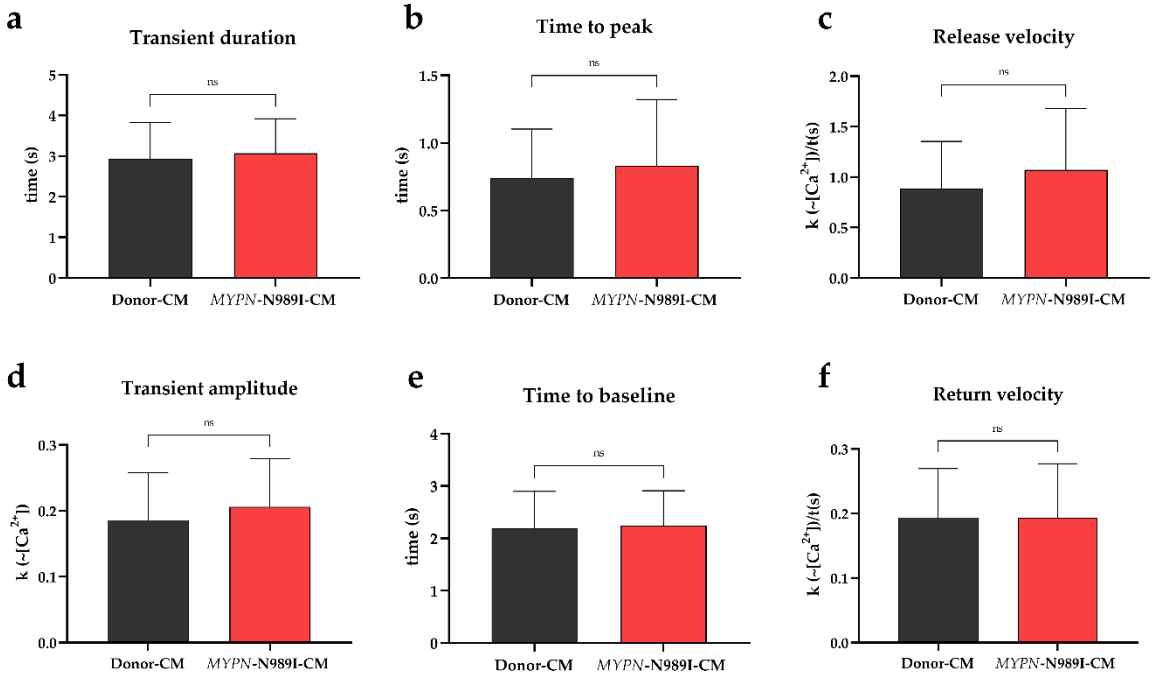

Figure 3. Parameters of calcium transients in iPSC-derived cardiomyocytes of the HCM patient and healthy donor. Black columns — healthy donor CMs (n>60); red columns — *MYPN*-N989I-CMs (n>90). (**a**) Duration of calcium transient; (**b**) Time to transient's peak; (**c**) Calcium rise velocity; (**d**) Amplitude of calcium transient; (**e**)

© 2025 by the author(s). Distributed under a Creative Commons CC BY license.

Preprints.org (www.preprints.org) | NOT PEER-REVIEWED | Posted: 22 December 2025 doi:10.20944/preprints202512.1808.v1

Time from peak to baseline; (**f**) Calcium decay velocity. p-value: ns – not significant. The data are presented as mean ± SD.

2.4. MYPN-N989I-Cardiomyocytes Do Not Demonstrate Any Significant Changes in Characteristics of Sodium Current and Action Ponential

To explore biophysical characteristics of sodium current in *MYPN*-N989I-CMs, we used patch-clamp technique. Both Donor-CMs and *MYPN*-N989I-CMs demonstrated typical sodium current traces (Figure 4a). No significant changes were observed in peak sodium current density in *MYPN*-N989I-CMs versus Donor-CMs (Figure 4b,c, Table 1). Next, we analyzed steady-state activation and steady-state inactivation properties (Figure 4d,e, Table1). We found a statistically significant depolarizing shift of 4 mV in the half-voltage of steady-state activation (Table 1). Thus, *MYPN*-N989I-CMs required more depolarization stimuli to action potential initiation and demonstrated features of sodium channel loss-of-function phenotype. In contrast, no statistically significant alteration of the steady-state inactivation was observed (Figure 4e, Table 1).

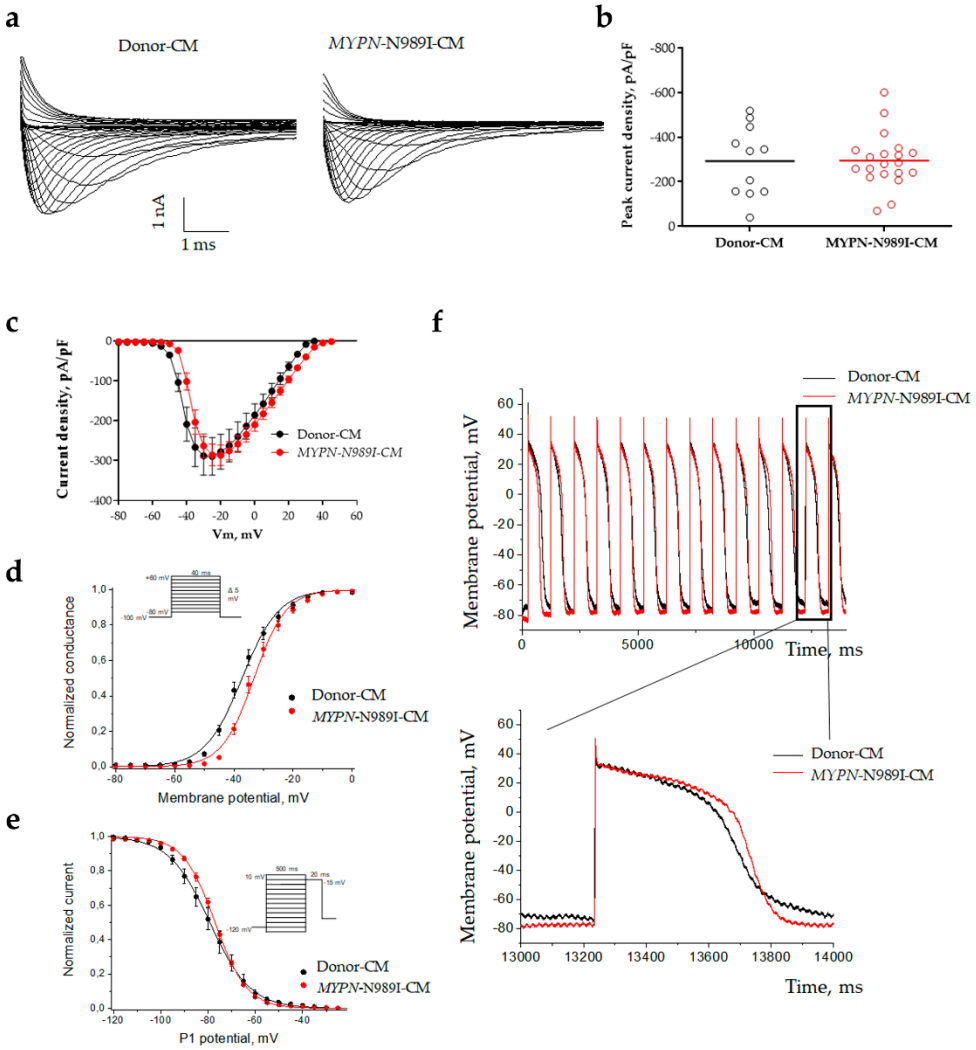

Figure 4. Sodium current parameters and action potential dynamics in iPSC-derived cardiomyocytes of the healthy donor (black) and HCM patient (red). (**a**) Representative sodium current traces; (**b**) Peak current density; (**c**) Voltampere characteristics of current density; (**d**) Steady-state activation of sodium current; (**e**) Steady-state inactivation of sodium current; (**f**) Action potential dynamics.

© 2025 by the author(s). Distributed under a Creative Commons CC BY license.

Preprints.org (www.preprints.org) | NOT PEER-REVIEWED | Posted: 22 December 2025 doi:10.20944/preprints202512.1808.v1

Table 1. Biophysical characteristics of sodium current. Data are represented as mean ± SEM.

		Donor-CMs	n	*MYPN*-N989I-CMs	n	p
Current density at -20mV	pA/pF	-292.1 ± 47.9	11	-294.5 ± 27.0	20	0.9506
Steady-state activation	$V_{1/2}$, mV	-37.1 ± 1.1	11	-33.1 ± 0.9	20	0.0121
	k	5.7 ± 0.3		4.6 ± 0.2		0.0194
Steady-state inactivation	$V_{1/2}$, mV	-79.2 ± 2.0	10	-77.1 ± 0.7	20	0.3012
	k	7.7 ± 0.5		6.5 ± 0.2		0.0114

We also studied the action potentials in *MYPN*-N989I-CMs and Donor-CMs to clarify the impact of the observed activation shift (Figure 4f). No changes in action potential duration and amplitude were detected (Table 2). Thus, despite the slightly impaired activation in *MYPN*-N989I-CMs, their overall electrical activity demonstrates no alterations.

Table 2. Action potential parameters. Data are represented as mean ± SEM.

	Donor-CMs, n=12	*MYPN*-N989I-CMs, n=9	p
APA, mV	130,2 ± 5,876	125,0 ± 3,314	0,6187
APD90, ms	572,6 ± 52,65	546,8 ± 54,58	0,859
APD70, ms	472,0 ± 47,57	459,5 ± 46,29	0,9717
APD30, ms	338,8 ± 37,13	318,8 ± 42,18	0,594

2.5. iPSC-Derived Cardiomyocytes with p.N989I Variant in MYPN Revealed a Dysregulation of Several Signaling Pathways

To further study the impact of the p.N989I (c.2966A>T) variant in *MYPN* on cardiocyomyte properties, we performed transcriptome analysis of *MYPN*-N989I-CMs and Donor-CMs using RNA sequencing technology. *MYPN*-N989I-CMs and Donor-CMs could be clearly divided by the principal component analysis (Figure 5a). Differential expression analysis revealed 424 significantly upregulated genes (DEGs) and 226 downregulated DEGs in *MYPN*-N989I-CMs compared to Donor-CMs (Figure 5b). To investigate the functional relevance of the detected DEGs, GO analysis using the Gene Ontology database (Biological Process, Cellular Components, Molecular Function) was performed. Significantly upregulated DEGs included genes involved in regulation of muscle system process, cell cycle and microtubule cytoskeleton organization (Figure 5c, Table 3). Among genes involved in muscle system process pathway the following genes were detected: *CASQ1, MYOM2, P2RX1, MYLK, SMTN, KCNJ8, CHRNA3, GATA5, TNNT3, TNNI3K, OXTR, KBTBD13, ATP8A2, PIK3CG, TNFRSF1B, STRIT1, IGF1, EDNRB, TRIM72, ACTN3* (Figure 4d).

© 2025 by the author(s). Distributed under a Creative Commons CC BY license.

Preprints.org (www.preprints.org) | NOT PEER-REVIEWED | Posted: 22 December 2025 doi:10.20944/preprints202512.1808.v1

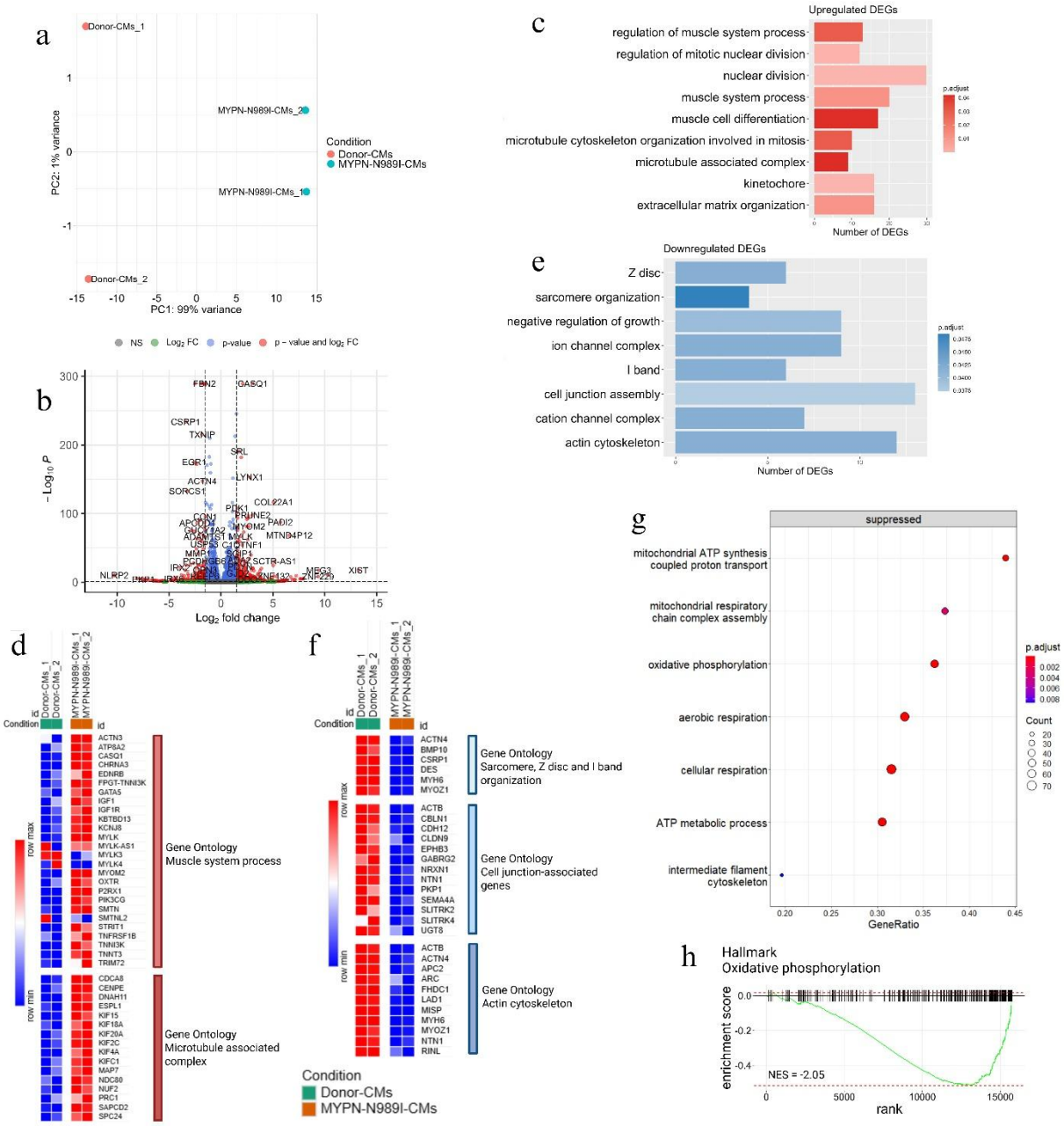

Figure 5. Transcriptome analysis of *MYPN*-N989I-CMs compared to Donor-CMs. (**a**) PCA plot; (**b**) Volcano-plot of differentially expressed genes (DEGs, |LFC| > 1.5 and p.adj < 0.05); (**c**) Gene set enrichment analysis of upregulated DEGs (p.adj < 0.05); (**d**) Heatmap of genes involved in Muscle system process and Microtubule associated complex signaling pathways; (**e**) Gene set enrichment analysis of downregulated DEGs (p.adj < 0.05); (**f**) Heatmap of genes involved in Sarcomere, Z-disc and I-band organization, Cell junction-associated genes and Actin cytoskeleton signaling pathways; (**g**) Results of FGSEA analysis; (**h**) GSEA plot of the Oxidative phosphorylation signaling pathways from Hallmark Gene Ontology database (NES = -2.05 and p.adj < 0.05).

Enrichment analysis revealed upregulation of cell cycle signaling pathways such as nuclear division, regulation of mitotic nuclear division and cell cycle checkpoint. Cyclin-dependent kinase 1 (*CDK1*) was among the genes involved in these pathways – its expression was increased in *MYPN*-N989I-CMs. Interestingly, in *MYPN*-N989I-CMs we detected the concominant decrease in the expression of *CDKN1A* (p21) gene - an inhibitor of CDK1. Among other genes linked to cell cycle signaling pathway there were genes responsible for formation of Ndc80 complex and structuring the division spindle, such as *NDC80*, *NUF2* and *SPC24*. In addition, *MYPN*-N989I-CMs demonstrated activation of genes involved in microtubule-kinetochore conjugation, microtubule assemble and

© 2025 by the author(s). Distributed under a Creative Commons CC BY license.

Preprints.org (www.preprints.org) | NOT PEER-REVIEWED | Posted: 22 December 2025 doi:10.20944/preprints202512.1808.v1

microtubule associated complex such as *KIF4A*, *NDC80*, *KIFC1*, *NUF2*, *CENPE*, *CDCA8*, *ESPL1*, *KIF15*, *PRC1*, *SAPCD2*, *DNAH11*, *KIF20A*, *KIF4A*, *KIFC1*, *KIF2C*, *KIF18A*, *CDCA8*, *MAP7*, *KIF15* (Figure 5d, Table 3).

Pathway analysis on downregulated DEGs revealed disturbances in sarcomere organization, Z-disc and I-band organization (*MYH6*, *DES*, *CSRP1*, *ACTN4*, *MYOZ1*, *BMP10*), cell junction-associated genes (*EPHB3*, *SEMA4A*, *NRXN1*, *GABRG2*, *PKP1*, *CBLN1*, *CDH12*, *SLITRK4*, *SLITRK2*, *UGT8*, *CLDN9*) as well as actin cytoskeleton (*ACTB*, *MYH6*, *ACTN4*, *MYO1D*, *LAD1*, *NTN1*, *MYOZ1*, *APC2*, *ARC*, *RINL*, *FHDC1*, *MISP*) (Figure 5 e, f, Table 3).

Table 3. Differently expressed genes from the detected signalling pathways.

Signaling pathway	Gene symbol	Gene name	LFC	p.adj
Muscle system process	*ACTN3*	actinin alpha 3	2.24	$3.91*10^{-2}$
	ATP8A2	ATPase phospholipid transporting 8A2	1.83	$6.62*10^{-4}$
	CASQ1	calsequestrin 1	3.06	0
	CHRNA3	cholinergic receptor nicotinic alpha 3 subunit	1.66	$4.57*10^{-22}$
	EDNRB	endothelin receptor type B	4.29	0.01
	GATA5	GATA binding protein 5	1.55	$1.62*10^{-8}$
	IGF1	insulin like growth factor 1	1.92	$6.24*10^{-3}$
	KBTBD13	kelch repeat and BTB domain containing 13	2.38	$7.47*10^{-5}$
	KCNJ8	potassium inwardly rectifying channel subfamily J member 8	1.57	$6.09*10^{-27}$
	MYLK	myosin light chain kinase	1.90	$1.66*10^{-67}$
	MYOM2	myomesin 2	2.70	$3.46*10^{-82}$
	OXTR	oxytocin receptor	2.19	$2.75*10^{-5}$
	P2RX1	purinergic receptor P2X 1	1.55	$9.67*10^{-81}$
	PIK3CG	phosphatidylinositol-4,5-bisphosphate 3-kinase catalytic subunit gamma	6.38	$1.84*10^{-4}$
	SMTN	smoothelin	1.55	$3.28*10^{-40}$
	STRIT1	small transmembrane regulator of ion transport 1	6.16	$4.03*10^{-3}$
	TNFRSF1B	TNF receptor superfamily member 1B	1.99	$3.96*10^{-3}$
	TNNI3K	TNNI3 interacting kinase	1.83	$1.03*10^{-6}$
	TNNT3	troponin T3, fast skeletal type	3.13	$9.81*10^{-8}$
	TRIM72	tripartite motif containing 72	1.65	0.02
Microtubule associated complex	*CDCA8*	cell division cycle associated 8	1.51	$2.35*10^{-6}$
	CENPE	centromere protein E	1.52	$1.21*10^{-6}$
	DNAH11	dynein axonemal heavy chain 11	5.04	$2.64*10^{-25}$
	ESPL1	extra spindle pole bodies like 1, separase	1.68	$3.59*10^{-5}$
	KIF15	kinesin family member 15	1.64	$4.95*10^{-3}$
	KIF18A	kinesin family member 18A	2.00	$3.19*10^{-7}$
	KIF20A	kinesin family member 20A	1.67	$1.61*10^{-15}$
	KIF2C	kinesin family member 2C	1.71	$2.67*10^{-9}$
	KIF4A	kinesin family member 4A	1.86	$8.12*10^{-13}$
	KIFC1	kinesin family member C1	1.80	$4.95*10^{-10}$
	MAP7	microtubule associated protein 7	1.59	$2.68*10^{-3}$
	NDC80	NDC80 kinetochore complex component	2.32	$1.50*10^{-11}$
	NUF2	NUF2 component of NDC80 kinetochore complex	2.27	$1.49*10^{-9}$
	PRC1	protein regulator of cytokinesis 1	2.18	$1.43*10^{-2}$
	SAPCD2	suppressor APC domain containing 2	1.56	0.02
	SPC24	kinetochore-associated Ndc80 complex subunit SPC24	1.59	$1.06*10^{-5}$

© 2025 by the author(s). Distributed under a Creative Commons CC BY license.

Preprints.org (www.preprints.org) | NOT PEER-REVIEWED | Posted: 22 December 2025 doi:10.20944/preprints202512.1808.v1

Sarcomere, Z-disc and I-band organization	*ACTN4*	actinin alpha 4	-1.79	$4.7*10^{-148}$
	BMP10	bone morphogenetic protein 10	-5.37	$4.91*10^{-2}$
	CSRP1	cysteine and glycine rich protein 1	-3.40	$1.86*10^{-234}$
	DES	desmin	-1.51	$4.73*10^{-289}$
	MYH6	myosin heavy chain 6	-1.95	0
	MYOZ1	myozenin 1	-1.68	$1.11*10^{-24}$
Cell junction associated genes	*ACTB*	actin beta	-1.81	0
	CBLN1	cerebellin 1 precursor	-1.70	$1.83*10^{-3}$
	CDH12	cadherin 12	-3.26	$5.18*10^{-3}$
	CLDN9	claudin 9	-1.66	0.04
	EPHB3	EPH receptor B3	-1.56	$1.75*10^{-81}$
	GABRG2	gamma-aminobutyric acid type A receptor subunit gamma2	-7.74	$1.81*10^{-5}$
	NRXN1	neurexin 1	-1.71	$5.66*10^{-7}$
	NTN1	netrin 1	-1.97	$3.61*10^{-63}$
	PKP1	plakophilin 1	-7.47	$5.99*10^{-5}$
	SEMA4A	semaphorin 4A	-2.48	$3.31*10^{-12}$
	SLITRK2	SLIT and NTRK like family member 2	-5.83	0.02
	SLITRK4	SLIT and NTRK like family member 4	-1.58	0.01
	UGT8	UDP glycosyltransferase 8	-1.81	0.04
Actin cytoskeleton	*ACTB*	actin beta	-1.81	0
	ACTN4	actinin alpha 4	-1.79	$4.67*10^{-148}$
	APC2	APC regulator of Wnt signaling pathway 2	-3.62	$4.09*10^{-5}$
	ARC	activity regulated cytoskeleton associated protein	-3.93	$1.94*10^{-4}$
	FHDC1	FH2 domain containing 1	-2.85	0.03
	LAD1	ladinin 1	-2.58	$6.27*10^{-75}$
	MISP	mitotic spindle positioning	-5.56	0.03
	MYH6	myosin heavy chain 6	-1.95	0
	MYO1D	myosin ID	-2.04	$7,09*10^{-91}$
	MYOZ1	myozenin 1	-1.68	$1.11*10^{-24}$
	NTN1	netrin 1	-1.97	$3.61*10^{-63}$
	RINL	Ras and Rab interactor like	-1.84	0.02

To deeper uncover transcriptomic signatures of *MYPN*-N989I-CMs, we also performed a fast gene set enrichment analysis (FGSEA) of non-DEGs using the Gene Ontology database. In addition to the previously described genes, this analysis revealed a suppression of signaling pathways associated with ATP synthesis, oxidative phosphorylation and cellular respiration (Figure 5g). FGSEA analysis using Hallmarks database also revealed downregulation of Oxidative Phosphorylation (Figure 5h).

To compare the changes observed at the transcriptomic level with earlier published data on other *MYPN*-defective cellular and animal models, we analyzed the expression of several Z-disc associated genes, genes related to Ca^{2+} homeostasis and genes involved in SRF-signaling pathway [2,3,5]. A decreased expression of *DES*, *DSP*, *VCL*, *PALLD* and *SORBS2* and an increased *ANKRD1* expression were detected (Figure 6a). We also observed the increased level of *CASQ1* and *CASQ2* in *MYPN*-N989I-CMs compared to Donor-CMs (Figure 6a). In addition, a marked downregulation of genes related to endoplasmic reticulum and calcium homeostasis and upregulation of genes related to sarcoplasmatic reticulum ion transport were detected in line with *CASQ1* and *CASQ2* upregulation (Figure 6b). Thus, we were able to confirm changes in the expression level for many earlier reported genes including those involved in SRF-signaling pathway (Figure 6c).

© 2025 by the author(s). Distributed under a Creative Commons CC BY license.

Preprints.org (www.preprints.org) | NOT PEER-REVIEWED | Posted: 22 December 2025 doi:10.20944/preprints202512.1808.v1

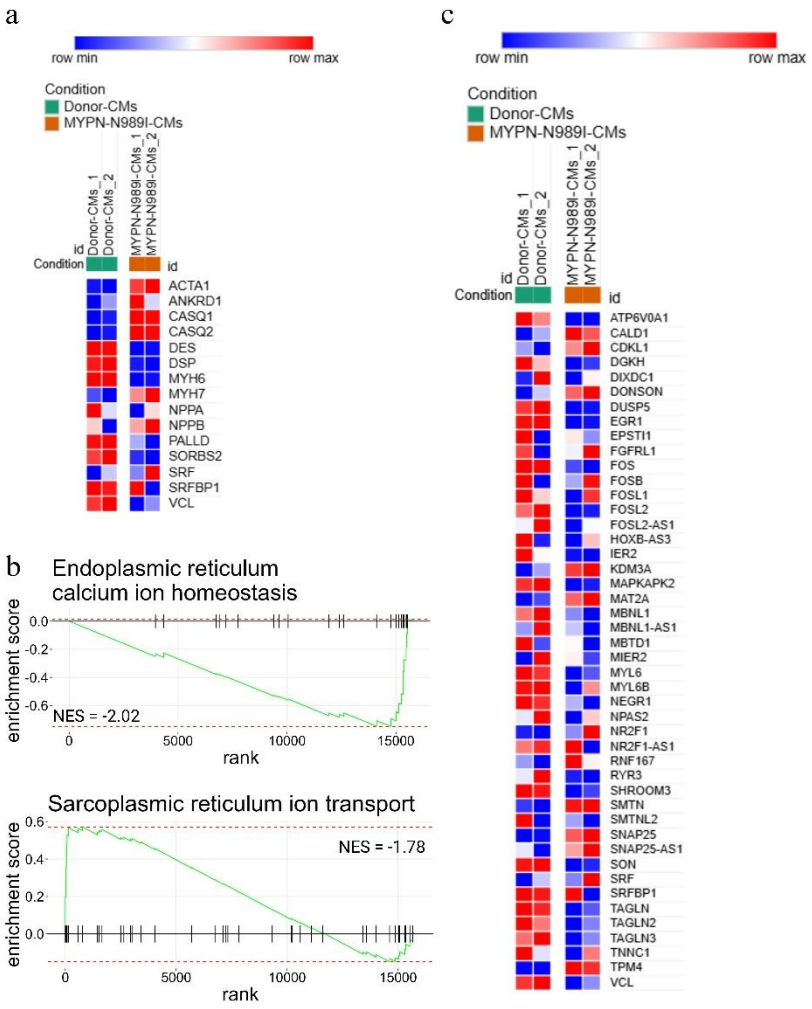

Figure 6. (**a**) Heatmap of Z-disc-associated genes and genes related to Ca^{2+} homeostasis; (**b**) GSEA plot of the Endoplasmic and Sarcoplasmic reticulum calcium ion homeostasis signaling pathways from Hallmark Gene Ontology database (NES = -2.02, NES = -1.78 and p.adj < 0.05).; (**c**) Heatmap of genes involved in SRF-signaling pathway.

To sum up, *MYPN*-N989I-CMs demonstrate significant upregulation of myogenic program, activation of cell cycle- and division spindle-linked genes, which may contribute to the development of cardiac hypertrophy, along with downregulation of sarcomeric, Z-disc- and cell junction-associated genes as well as ATP synthesis, oxidative phosphorylation-related genes and genes involved in SRF-signaling pathway.

3. Discussion

Mutations in *MYPN* gene have been demonstrated in connection to various human pathologies since 2008 first being described in patients with dilated cardiomyopathy and later in other types of cardiomyopathies - hypertrophic and restrictive [6,8,29,30]. Along with cardiac disorders, *MYPN* loss of function or homozygous mutations were reported in congenital and slow-progressive myopathies – similar to other genes commonly expressed in cardiac and skeletal muscle. However, there are still some difficulties in the interpretation of pathogenic role of *MYPN* variants, especially since they are often detected not solely, but in combination with other pathogenic variants and not always clearly segregate with the disease [4,31]. Apart from the causative role of *MYPN* in monogenic cardiac and neuromuscular disorders, this gene was described as one of the genetic loci associated with atrial fibrillation and cardiac remodelling [32,33]. All above rise the need for more detailed knowledge on the fine molecular mechanisms of *MYPN*-associated pathologies and the bases for *MYPN*-linked

© 2025 by the author(s). Distributed under a Creative Commons CC BY license.

Preprints.org (www.preprints.org) | NOT PEER-REVIEWED | Posted: 22 December 2025 doi:10.20944/preprints202512.1808.v1

cardiomyocyte dysfunction. The described substitution p.N989I (c.2966A>T) is located in the third Ig domain of MYPN. In myopalladin homologue, palladin (PLLD), this region is important for direct binding interaction with F-actin [23]. It is possible that substitutions in a similar region of myopalladin can also lead to changes in actinin binding or interfere with protein-protein interactions, leading to functional and adaptive transcriptional changes. To address this question, we created the first iPSC-derived cardiomyocyte cellular model to search for ion channel dysfunction, calcium homeostasis abnormalities and alterations in gene expression profile due to a novel HCM-associated *MYPN*-N989I variant.

MYPN function is mainly demonstrated in connection to mechanotransduction process within sarcomeric Z-line and I-band. In a tight connection with ANKRD1 (CARP), ANKRD2, TTN, actinin 2, nebulette and some other Z-line-associated proteins, MYPN facilitates the transformation of mechanical stimuli from contractile apparatus to biochemical signals and adapts the muscle cells to intrinsic and extracellular stress by activating various stress-response pathways and programs [1,3,34]. The potential interaction of MYPN with PDLIM5, LDB3, OBSCN and MYOM1 has also been proposed by a computational approach [35]. This tight incorporation into Z-disc structure makes the protein relevant to the development of protein-surplus skeletal myopathies such as slowly progressive nemaline myopathies. The mechanism underlying these pathologies is mainly based on the interaction disruption of MYPN with multiple Z-line associated binding partners and a “domino effect”. In addition to the structural role, the shuttling function between Z-line and the nucleus in tight interaction with ANKRD2 was demonstrated for MYPN, further supporting its role in mechanotransduction [29,36]. A possible involvement of MYPN in SRF-signaling pathways and ERK cascade regulation was also demonstrated by several research groups [3,29]. However, up and downregulated genes and the signaling pathways activated in response to MYPN mutations are often controversial and depend on the cell line and animal models used and, importantly, type of mutation and the length of the studied protein [2,3,29]. This may be attributed to the different interaction partners of MYPN within the nucleus and Z-line structure as well as different effects of loss-of function and dominant-negative mutations [5]. In spite of several published studies no clear functional consequences apart from the effect on sarcomeric structure and nuclear translocation of MYPN and its partners have been demonstrated for *MYPN* mutations [2,29].

In our study, we also failed to detect gross functional abnormalities in iPSC-derived cardiomyocytes neither in intracellular calcium dynamics and transients nor in voltage-dependent Nav1.5 sodium channel currents. The slight alteration in Nav1.5 kinetics in a form of depolarizing shift of steady-state activation and features of sodium channel loss-of-function phenotype, however, did not result in significant changes in action potential duration and amplitude, arguing for no remarkable effect of the HCM-associated *MYPN*-N989I variant on overall electrical activity of cardiomyocytes. However, in an earlier study by Filomena et al., authors demonstrated altered Ca^{2+} handling, namely a delayed Ca^{2+} release and reuptake as well as reduced Ca^{2+} spark amplitude and the velocity of Ca^{2+} release in *MYPN*-knockout (KO) mice. This difference needs some explanation in terms of MYPN function and effect on myocyte Ca^{2+} handling. First, it can be attributed to the different systems used in the studies: while Filomena and co-authors used knockout mouse model and performed Ca^{2+} release studies in the isolated cardiomyocytes with complete absence of MYPN, we used iPSC-derived cardiomyocytes carrying the heterozygous *MYPN*-N989I substitution. Knowing complex MYPN interactions with structural and regulating proteins, it is reasonable to suggest that one amino acid substitution is not enough to trigger the cascade of reactions leading to alterations in Ca^{2+} homeostasis while the total absence of MYPN can significantly influence Ca^{2+} handling via abnormal differentiation properties of cardiomyocytes and reduced protein-protein interactions. This mechanism was ealier reported for FLNC-knockout cells and, potentially, can be attributed to many actinin-binding structural proteins [37,38]. In addition, the difference in species-dependent properties – mouse adult cardiomyocytes and iPSC-derived human cardiomyocytes can also explain the observed differences.

© 2025 by the author(s). Distributed under a Creative Commons CC BY license.

Preprints.org (www.preprints.org) | NOT PEER-REVIEWED | Posted: 22 December 2025 doi:10.20944/preprints202512.1808.v1

In spite of scare functional changes detected in *MYPN*-N989I-CMs we were able to detect significant differences in gene expression profile compared to Donor-CMs. Significant alterations in pathways and processes associated with regulation of muscle system process, differentiation and cell nuclear division along with microtubule cytoskeleton organization correspond to earlier reported data obtained on muscle tissue of *MYPN*-KO mice [3]. This goes along with a downregulation of Z-disc and sarcomere organisation and actin cytoskeleton associated proteins reported by the same authors, further supporting the role of MYPN in driving myogenic program (Figure 10 from [3]). Of note, in *MYPN*-N989I-CMs, we detected an upregulation of *ANKRD1* similar to that reported earlier by Filomena and co-authors for *MYPN*-KO skeletal muscle cells and cardiomyocytes and detected by RNA sequencing and real-time PCR [2,3]. The similar observation is valid for *PALLD* which downregulation was registered both in our and previous studies [2,3]. We suggest that the pathogenic effect of *MYPN*-N989I variant in terms of *ANKRD1* and *PALLD* regulation is similar to MYPN ablation and, possibly, can be linked to the altered protein-protein interactions. Defective interaction of MYPN and ANKRD1 can cause the decreased shuttling and translocation of ANKRD1 to the nucleus, thus, consequently leading to its upregulation [3,5].

Using RNA sequencing, we also confirmed a downregulation of *DES*, *DSP* and *VCL* in *MYPN*-N989I-CMs – similar to that detected on a protein level in transgenic *MYPN*-Y20C mice and, in addition, demonstrated *SORBS2* downregulation, further underscorring the role of MYPN in Z-disc, desmosome and cell-contact organisation [5]. We managed to confirm the alterations in mitochondrial respiration and ATP-production processes in *MYPN*-N989I-CMs – an observation reported earlier at the ultrastructural level in human *MYPN*-Q529X cardiomyocytes [5]. These findings independently verified in different experimental systems, cell types and for various *MYPN* mutations provide a strong evidence for MYPN involvement in both Z-disc and cytoskeletal organisation, structure and regulation of cellular contacts and mitochondrial function. In addition, in spite of no functional changes in Ca^{2+} transients we detected a marked derangements in genes related to calcium homeostasis at the transcriptional level. Thus, *MYPN*-N989I interferes with calcium-homeostasis related genes – an observation alining with *MYPN*-KO-related alterations in calcium oscillation in cardiomyocytes [2]. Importantly, we also were able to confirm the downregulation of the SRF-pathway in *MYPN*-N989I-CMs – phenomenon described for *MYPN*-KO skeletal muscle cells [3], further supporting the role of MYPN in transcriptional regulation, possibly, through interaction with actin cytoskeleton and ANKRD1. Thus, we deliniated a dual role of MYPN both in sarcomeric and cytoskeletal organisation as well as in muscle program regulation.

4. Materials and Methods

4.1. Sequence and Structural Analysis of Human Myopalladin and Variant Classification

Sequence for the human myopalladin was obtained from the UniProtKB database under the entry Q86TC9. Domain organization of the protein was performed using InterPro database [24] and lollipops tool [25]. Related protein sequences from other organisms for myopalladin were identified by BLASTP [39] search against the Uniref90 database. Similar Ig regions in other human proteins were identified using human proteome (UniProt ID: UP000005640). Multiple sequence alignment was calculated by Clustal Omega [40] and visualized in Jalview 2.11.5 [41]. 3D structure of the Ig-like domain of myopalladin (PDB: 2LQR, chain A) [23] was extracted from the Protein Data Bank [42,43]. Variant p.N989I was mapped on the structure according to the sequence alignment. In silico visualization was conducted using the PyMol 2.5 software. Pathogenicity of variant p.N989I was assessed based on the ClinPred and AlphaMissense prediction scores obtained from the dbNSFP database version 4.5 [44].

© 2025 by the author(s). Distributed under a Creative Commons CC BY license.

Preprints.org (www.preprints.org) | NOT PEER-REVIEWED | Posted: 22 December 2025 doi:10.20944/preprints202512.1808.v1

4.2. iPSC Generation

8.1 × 10^5 of mononuclear cells (MNCs) of the HCM patient carrying p.N989I (c.2966A>T) variant in *MYPN* were electroporated with episomal vectors (0.5 μg each, Addgene IDs #41855-41858, #41813-41814) using Neon Transfection System (Thermo Fisher Scientific, Waltham, MA, USA), program: 1650 V, 10 ms, 3 times. All reprogramming steps were performed according to the Epi5™ Episomal iPSC Reprogramming Kit user guide (Thermo Fisher Scientific, Waltham, MA, USA). Primary iPSC colonies were picked manually, transferred on a feeder layer, and maintained in KnockOut DMEM supplemented with 15% KnockOut Serum Replacement (KoSR), 0.1 mM Non-Essential Amino Acid (NEAA), 1× penicillin-streptomycin, 1 mM GlutaMAX (all Thermo Fisher Scientific, Waltham, MA, USA), 0.05 mM 2-mercaptoethanol (Amresco, Solon, OH, USA), and 10 ng/ml bFGF (SCI-store, Moscow, Russia). Cells were cultured at 37°C in 5% CO_2 and passaged at a ratio of 1:10 every 3-5 days with TrypLE™ Express Enzyme (Thermo Fisher Scientific, Waltham, MA, USA).

4.3. Mycoplasma and Episome Detection

Mycoplasma contamination and episome elimination in iPSC lines were detected by PCR on a T100 Thermal Cycler (Bio-Rad, Hercules, CA, USA) with BioMaster HS-Taq PCR-Color (2×) (Biolabmix, Novosibirsk, Russia). Programs: 95°C – 3 min; 35 cycles: 95°C – 15 s, 67°C – 15 s, 72°C – 20 s; 72°C – 5 min (mycoplasma) and 95°C – 5 min; 35 cycles: 95°C – 15 s, 62°C – 15 s, 72°C – 15 s; 72°C – 5 min (episomes). The primers used are given in Table S1.

4.4. Spontaneous In Vitro Differentiation

iPSCs were dissociated with 0.15% Collagenase Type IV (Thermo Fisher Scientific, Waltham, MA, USA), transferred onto dishes coated with 1% agarose, and cultivated for 14 days in DMEM/F12 (1:1) medium supplemented with 15% KoSR, 0.1 mM NEAA, 1× penicillin-streptomycin, 1 mM GlutaMAX (all Thermo Fisher Scientific, Waltham, MA, USA). The embryoid bodies formed were plated onto Matrigel (Corning, New York, NY, USA)-coated 8-well Chambered Coverglass (Thermo Fisher Scientific, Waltham, MA, USA) for additional seven days.

4.5. Immunofluorescent Staining

Cells were fixed in 4% paraformaldehyde (Sigma-Aldrich, Darmstadt, Germany) for 10 min, permeabilized in 0.4% Triton-X100 (Sigma-Aldrich, Darmstadt, Germany) for 10 min, incubated with 1% BSA (VWR, Solon, OH, USA) for 30 min. Cells were incubated overnight at 4°C with primary antibodies and 1h at room temperature with secondary antibodies. The antibodies used are listed in Table S1. After each incubation with antibodies, the cells were washed twice for 15 min with PBS. Nuclei were counterstained with DAPI (Sigma-Aldrich, Darmstadt, Germany). Staining was analyzed using a Nikon Eclipse Ti-E microscope and NIS Elements software (Nikon, Tokyo, Japan) or Observer.Z1 and ZEISS Efficient Navigation (ZEN) (Zeiss, Oberkochen, Germany).

4.6. RT-qPCR

RNA was isolated with TRIzol Reagent (Thermo Fisher Scientific, Waltham, MA, USA) according to the manufacturer's protocol. Reverse transcription of 1-2 μg of RNA was performed with the M-MuLV reverse transcriptase (Biolabmix, Novosibirsk, Russia). RT-qPCR was carried out on a LightCycler 480 System (Roche, Basel, Switzerland) with BioMaster HS-qPCR SYBR Blue 2× (Biolabmix, Novosibirsk, Russia). Program: 95°C – 5 min; 40 cycles: 95°C – 10 s, 60°C – 1 min. CT values were normalized to *ACTB* using ΔΔCT method. The primers used are given in Table S1.

4.7. Karyotyping

Colcemid treatment, cell hypotony and fixation were carried out as described previously [45]. Karyotype was analyzed at the Tomsk National Research Medical Center of the Russian Academy of

© 2025 by the author(s). Distributed under a Creative Commons CC BY license.

Preprints.org (www.preprints.org) | NOT PEER-REVIEWED | Posted: 22 December 2025 doi:10.20944/preprints202512.1808.v1

Sciences using a Zeiss Axio Scope.A1 microscope (Zeiss, Oberkochen, Germany) and Ikaros KARyOtyping Software (MetaSystems, Altlussheim, Germany).

4.8. Analysis of the Patient-Specific Variant

Exon 14 of *MYPN* was amplified by PCR on a T100 Thermal Cycler (Bio-Rad, Hercules, CA, USA) with BioMaster HS-Taq PCR-Color (2×) (Biolabmix, Novosibirsk, Russia). Program: 95°C – 5 min; 35 cycles: 95°C – 30 s, 60°C – 30 s, 72°C – 30 s; 72°C – 5 min. The primers used are given in Table S1. Sanger sequencing was performed using Big Dye Terminator V. 3.1. Cycle Sequencing Kit (Applied Biosystems, Austin, TX, USA) and analyzed at the SB RAS Genomics Core Facility.

4.9. STR Analysis

STR analysis of the patient-specific iPSC lines and MNCs was performed by Genoanalytica (https://www.genoanalytica.ru) using COrDIS EXPERT 26 Kit (Gordiz, Moscow, Russia) on a 3130 Genetic Analyzer (HITACHI, Applied Biosystems, Japan).

4.10. Directed iPSC Differentiation into Cardiomyocytes

iPSCs were cultivated for 2-3 passages in feeder-free conditions - in Essential 8 Medium (Thermo Fisher Scientific, Waltham, MA, USA) on wells coated with Geltrex LDEV-Free hESC-Qualified Reduced Growth Factor Basement Membrane Matrix (Thermo Fisher Scientific, Waltham, MA, USA). iPSCs were dissociated with ReLeSR (STEMCELL Technologies, Vancouver, BC, Canada) and plated at a ratio of 1:5-1:10 on 12-well plates. After cells reached 80-90% confluency, differentiation was induced by adding for 48h RPMI 1640 medium supplemented with 1× penicillin-streptomycin, 1× B27 Supplement minus insulin (all Thermo Fisher Scientific, Waltham, MA, USA) and 6 μM CHIR99021 (Selleckchem, Houston, TX, USA). 72 h after differentiation onset, RPMI 1640 medium supplemented with 1× penicillin-streptomycin, 1× B27 Supplement minus insulin and 5 μM IWR1 (STEMCELL Technologies, Vancouver, BC, Canada) was added for another 48h. Starting from day 7 of differentiation, cells were cultivated in RPMI 1640 medium supplemented with 1× penicillin-streptomycin and 1× B27 Supplement (Thermo Fisher Scientific, Waltham, MA, USA).

On day 9 of differentiation, cells were subjected to metabolic selection for 6 days in RPMI 1640 medium without D-glucose (Thermo Fisher Scientific, Waltham, MA, USA) supplemented with 1× penicillin-streptomycin, 213 μg/ml L-ascorbic acid 2-phosphate sesquimagnesium salt hydrate, 500 μg/ml bovine serum albumin and 5 mM sodium DL-lactate (all Sigma-Aldrich, Darmstadt, Germany). Cardiomyocytes were dissociated with 2.5× TrypLE™ Select Enzyme (Thermo Fisher Scientific, Waltham, MA, USA), plated on Geltrex-coated 6-well plates and cultivated for two weeks in RPMI 1640 medium supplemented with 1× penicillin-streptomycin, 1× B27 Supplement and 2 μM CHIR99021. On day 30 of differentiation, cardiomyocytes were plated on Geltrex-coated 12-well plates at a ratio of 9×10^5 - 1×10^6 cells per well. Cells were cultivated for two weeks in the medium for cardiomyocyte maturation [28] - DMEM without D-glucose and L-glutamine (Thermo Fisher Scientific, Waltham, MA, USA) supplemented with 3 mM glucose, 10 mM L-lactate, 5 μg/ml Vitamin B12, 0.82 μM Biotin, 5 mM Creatine monohydrate, 2 mM Taurine, 2 mM L-carnitine, 0.5 mM L-ascorbic acid 2-phosphate sesquimagnesium salt hydrate (all Sigma-Aldrich, Darmstadt, Germany), 0.1 mM NEAA, 1× B27 Supplement, 1% KoSR, 1× penicillin-streptomycin, 2 mM L-glutamine and 0.5% (w/v) Albumax (all Thermo Fisher Scientific, Waltham, MA, USA).

4.11. Calcium Dynamic with STIMULATION

Registration of calcium transients was performed with electrical stimulation using IonOptix setup (IonOptix, Westwood, MA, USA). Calcium measurements were registered using calcium-sensitive fluorescent dye Fura-2AM (Thermo Fisher Scientific, Waltham, MA, USA) and analyzed values constituted the fluorescence ratio between Fura-2AM channels (binding calcium or not). Cells were seeded on Geltrex-treated 170 μm thick coverglasses (Thermo Fisher Scientific, Waltham, MA,

© 2025 by the author(s). Distributed under a Creative Commons CC BY license.

Preprints.org (www.preprints.org) | NOT PEER-REVIEWED | Posted: 22 December 2025 doi:10.20944/preprints202512.1808.v1

USA), pre-washed with PBS to remove the medium and incubated with 2 μM Fura-2AM in calcium-containing buffer (145 mM NaCl, 4.5 mM KCl, 2 mM $MgCl_2$, 10 mM HEPES; 2 mM $CaCl_2$) for 40 minutes prior to imaging. Cells were paced at 0.2 Hz with a 10V square pulse using a MyoPacer field stimulator (IonOptix, Westwood, MA, USA). The images for each cell were recorded during 2–3 minutes and the transients for one cell were pooled and averaged. Data was recorded from each dish for no more than 30 minutes to avoid cell death.

4.12. Electrophysiology

Sodium currents and action potentials were recorded using whole-cell patch-clamp configuration at room temperature. For patch-clamp measurements, single cardiomyocytes were seeded on Geltrex-coated coverslips. We used the solutions described earlier [46] with a slight modification in the extracellular solution (50 mM NaCl and 90 mM CsCl instead of 140 mM NaCl).

Microelectrodes were manufactured using a puller (P-1000, Sutter Instrument, Novato, CA, USA). The electrode resistance ranged from 2.0 to 3.5 MΩ. Data acquisition and junction potential correction were done using Axopatch 200B amplifier and Clampfit software version 10.3 (Molecular Devices, San Jose, CA, USA). Currents were acquired at 20–50 kHz and low-pass filtered at 5 kHz using an analog-to-digital interface (Digidata 1440A acquisition system, Molecular Devices, San Jose, CA, USA). The series resistance was compensated at 75–80%. All pulse protocols were applied more than 5 min after membrane rupture. APs were elicited at 1 Hz by 3 ms, 1.2× threshold current pulses through the patch pipette.

4.13. Patch-Clamp Data Analyses

Pulse protocols were applied with a holding potential of −100 mV. Current-voltage (I-V) curves were assessed by depolarizing voltage steps from −80 to 60 mV during 40 ms in 5 mV increments at 1 Hz frequency. Current densities at each test potential were obtained by dividing the INa by cell capacitance. Cell capacitance values did not differ significantly between experimental groups. The AP amplitude (APA) and AP duration (APD) at 30, 70 and 90% repolarization (APD30, APD70 and APD90, respectively) were analyzed using IgorPro8 software (WaveMetrics, Portland, OR, USA).

4.14. RNA Sequencing and Bioinformatics Analysis

RNA sequencing libraries were prepared using the TruSeq Stranded mRNA kit (Illumina, San Diego, CA, USA) following the manufacturer's guidelines. The libraries' quantity was assessed using the 4150 TapeStation system (Agilent, Santa Clara, CA, USA) with High Sensitivity DNA ScreenTape Analysis. Subsequently, sequencing was carried out on the Illumina NextSeq 2000 (100 cycles). The quality assessment of the raw reads was evaluated using the FastQC tool (v0.11.9), fastp program (v0.12.4) was used to remove overrepresented polyG sequences. Following this, the reads were aligned to the human genome using the STAR aligner (v2.7.9) with the GRCh38.p13 reference genome and the GENCODE annotation (gencode.v41.primary assembly). Mapped reads were count with the featureCounts program (v2.0.3). The identification of differentially expressed genes (DEGs) was carried out using the RStudio package DESeq2 (v1.40.1). The p-values of the genes were adjusted with the Benjamini-Hochberg procedure and filtered with p.adj < 0.05; only genes with a $|\log2 \text{ fold change}| \geq 1.5$ were considered as differentially expressed. Subsequently, Gene Set Enrichment Analysis and GO Enrichment Analysis of gene sets were performed to obtain signaling pathways using Gene Ontology database.

4.15. Statistics

At least three independent experiments (independent cardiac differentiations) were performed for each measurement. Statistical analysis was performed using GraphPad Prism version 5.00 for Windows. For comparison of two groups, the Mann–Whitney test was used. An alpha level of 0.05 was used for all statistical analyses. Data are presented as mean ± SD or mean ± SEM.

© 2025 by the author(s). Distributed under a Creative Commons CC BY license.

Preprints.org (www.preprints.org) | NOT PEER-REVIEWED | Posted: 22 December 2025 doi:10.20944/preprints202512.1808.v1

5. Conclusions

In the current study we aimed to decipher *MYPN*-associated pathogenetic mechanisms underlying hypertrophic cardiomyopathy. Using the iPSC-technology, we analyzed functional properties and gene expression pattern in cardiomyocytes with a novel p.N989I (c.2966A>T) variant in *MYPN*. Despite no significant alterations in parameters of calcium transients, sodium current and action potential were found, the p.N989I (c.2966A>T) variant in *MYPN* had a global impact on the transcriptomic profile of iPSC-derived cardiomyocytes. We observed an upregulation of genes linked to cell cycle, division sprindle, microtubule cytoskeleton organization and myogenic program genes as well as a downregulation of sarcomeric, Z-disc- and cell junction-associated genes. In addition, genes involved in ATP synthesis, oxidative phosphorylation and SRF-signaling pathway were also downregulated. Our results come in a good agreement with the previously published data obtained using different cell and animal models and *MYPN* variants. Together these shed more light on pathogenesis of MYPN-associated cardiomyopathies and myopathies, supporting MYPN role not only in sarcomeric and cytoskeletal organization but also in regulation of muscle gene program.

Supplementary Materials: The following supporting information can be downloaded at the website of this paper posted on Preprints.org, Figure S1: Cells obtained in the course of directed cardiac differentiation of the patient-specific iPSC lines, FAMRCi015-A and FAMRCi015-B, express a cardiomyocyte marker, cardiac troponin I, Table S1: Primers and antibodies used in this study.

Author Contributions: Conceptualization, A.A.K. and S.M.Z.; methodology, A.A.K. and S.M.Z.; data analysis and validation, E.V.D., E.S.K., M.Y.S., A.K.Z., M.T.R., E.G.N., A.M.Z., D.A.K., S.I.T., Y.V.V., D.N.S. and A.A.K.; investigation, E.V.D., E.S.K., M.Y.S., A.K.Z., E.G.N., A.M.Z., S.I.T.; resources, A.A.K. and S.M.Z.; writing—original draft preparation, E.V.D., M.Y.S., E.S.K., A.K.Z., M.T.R. and A.A.K.; writing—review and editing, A.A.K., E.V.D. and M.Y.S.; supervision and funding acquisition, A.A.K. All authors have read and agreed to the published version of the manuscript.

Funding: This research was funded by Ministry of Science and Higher Education of the Russian Federation (Agreement No. 075-15-2022-301) and the Russian Science Foundation, grant No. 25-15-00552.

Institutional Review Board Statement: The study was conducted according to the guidelines of the Declaration of Helsinki and approved by the Ethics Committee of the E.N. Meshalkin National Medical Research Center (Protocol No. 31 dated 28 June 2013).

Informed Consent Statement: Informed consent was obtained from all subjects involved in the study.

Data Availability Statement: The data on the iPSC line characterization are available in the Human Pluripotent Stem Cell Registry (https://hpscreg.eu/cell-line/FAMRCi015-A, https://hpscreg.eu/cell-line/FAMRCi015-B accessed on 12 August 2025). The raw RNA sequence data and counts table were submitted in the GEO database and are available under accession number GSE305865.

Acknowledgments: The analysis of immunofluorescence staining was performed using resources of the Common Facilities Centre of Microscopic Analysis of Biological Objects supported by the State project of ICG SB RAS (FWNR-2022-0015).

Conflicts of Interest: The authors declare no conflicts of interest.

References

1. Bang, M.L.; Mudry, R.E.; McElhinny, A.S.; Trombitás, K.; Geach, A.J.; Yamasaki, R.; Sorimachi, H.; Granzier, H.; Gregorio, C.C.; Labeit, S. Myopalladin, a novel 145-kilodalton sarcomeric protein with multiple roles in Z-disc and I-band protein assemblies. *J. Cell Biol.* **2001**, *153*, 413–427. https://doi.org/10.1083/jcb.153.2.413.
2. Filomena, M.C.; Yamamoto, D.L.; Carullo, P.; Medvedev, R.; Ghisleni, A.; Piroddi, N.; Scellini, B.; Crispino, R.; D'Autilia, F.; Zhang, J.; et al. Myopalladin knockout mice develop cardiac dilation and show a

© 2025 by the author(s). Distributed under a Creative Commons CC BY license.

Preprints.org (www.preprints.org) | NOT PEER-REVIEWED | Posted: 22 December 2025 doi:10.20944/preprints202512.1808.v1

maladaptive response to mechanical pressure overload. *Elife* **2021**, *10*, e58313. https://doi.org/10.7554/eLife.58313.

3. Filomena, M.C.; Yamamoto, D.L.; Caremani, M.; Kadarla, V.K.; Mastrototaro, G.; Serio, S.; Vydyanath, A.; Mutarelli, M.; Garofalo, A.; Pertici, I.; et al. Myopalladin promotes muscle growth through modulation of the serum response factor pathway. *J. Cachexia Sarcopenia Muscle* **2020**, *11*, 169–194. https://doi.org/10.1002/jcsm.12486.
4. Bagnall, R.D.; Yeates, L.; Semsarian, C. Analysis of the Z-disc genes PDLIM3 and MYPN in patients with hypertrophic cardiomyopathy. *Int. J. Cardiol.* **2010**, *145*, 601–602. https://doi.org/10.1016/j.ijcard.2010.08.004.
5. Purevjav, E.; Arimura, T.; Augustin, S.; Huby, A.C.; Takagi, K.; Nunoda, S.; Kearney, D.L.; Taylor, M.D.; Terasaki, F.; Bos, J.M.; et al. Molecular basis for clinical heterogeneity in inherited cardiomyopathies due to myopalladin mutations. *Hum. Mol. Genet.* **2012**, *21*, 2039–2053. https://doi.org/10.1093/hmg/dds022.
6. Meyer, T.; Ruppert, V.; Ackermann, S.; Richter, A.; Perrot, A.; Sperling, S.R.; Posch, M.G.; Maisch, B.; Pankuweit, S.; German Competence Network Heart Failure. Novel mutations in the sarcomeric protein myopalladin in patients with dilated cardiomyopathy. *Eur. J. Hum. Genet.* **2013**, *21*, 294–300. https://doi.org/10.1038/ejhg.2012.173.
7. Zhao, Y.; Feng, Y.; Zhang, Y.M.; Ding, X.X.; Song, Y.Z.; Zhang, A.M.; Liu, L.; Zhang, H.; Ding, J.H.; Xia, X.S. Targeted next-generation sequencing of candidate genes reveals novel mutations in patients with dilated cardiomyopathy. *Int. J. Mol. Med.* **2015**, *36*, 1479–1486. https://doi.org/10.3892/ijmm.2015.2361.
8. Duboscq-Bidot, L.; Xu, P.; Charron, P.; Neyroud, N.; Dilanian, G.; Millaire, A.; Bors, V.; Komajda, M.; Villard, E. Mutations in the Z-band protein myopalladin gene and idiopathic dilated cardiomyopathy. *Cardiovasc. Res.* **2008**, 77, 118–125. https://doi.org/10.1093/cvr/cvm015.
9. Vershinina, T.; Fomicheva, Y.; Muravyev, A.; Jorholt, J.; Kozyreva, A.; Kiselev, A.; Gordeev, M.; Vasichkina, E.; Segrushichev, A.; Pervunina, T.; et al. Genetic Spectrum of Left Ventricular Non-Compaction in Paediatric Patients. *Cardiology* **2020**, *145*, 746–756. https://doi.org/10.1159/000510439.
10. Lornage, X.; Malfatti, E.; Chéraud, C.; Schneider, R.; Biancalana, V.; Cuisset, J.M.; Garibaldi, M.; Eymard, B.; Fardeau, M.; Boland, A.; et al. Recessive MYPN mutations cause cap myopathy with occasional nemaline rods. *Ann. Neurol.* **2017**, *81*, 467–473. https://doi.org/10.1002/ana.24900.
11. Dementyeva, E.V.; Vyatkin, Y.V.; Kretov, E.I.; Elisaphenko, E.A.; Medvedev, S.P.; Zakian, S.M. Genetic analysis of patients with hypertrophic cardiomyopathy. *Genes and Cells* **2020**, *15*, 68–73. https://doi.org/10.23868/202011011.
12. Bhagwan, J.R.; Mosqueira, D.; Chairez-Cantu, K.; Mannhardt, I.; Bodbin, S.E.; Bakar, M.; Smith, J.G.W.; Denning, C. Isogenic models of hypertrophic cardiomyopathy unveil differential phenotypes and mechanism-driven therapeutics. *J. Mol. Cell. Cardiol.* **2020**, *145*, 43–53. https://doi.org/10.1016/j.yjmcc.2020.06.003.
13. Shafaattalab, S.; Li, A.Y.; Gunawan, M.G.; Kim, B.; Jayousi, F.; Maaref, Y.; Song, Z.; Weiss, J.N.; Solaro, R.J.; Qu, Z.; Tibbits, G.F. Mechanisms of Arrhythmogenicity of Hypertrophic Cardiomyopathy-Associated Troponin T (*TNNT2*) Variant I79N. *Front. Cell Dev. Biol.* **2021**, *9*, 787581. https://doi.org/10.3389/fcell.2021.787581.
14. Vander Roest, A.S.; Liu, C.; Morck, M.M.; Kooiker, K.B.; Jung, G.; Song, D.; Dawood, A.; Jhingran, A.; Pardon, G.; Ranjbarvaziri, S.; et al. Hypertrophic cardiomyopathy β-cardiac myosin mutation (P710R) leads to hypercontractility by disrupting super relaxed state. *Proc. Natl. Acad. Sci. U S A* **2021**, *118*, e2025030118. https://doi.org/10.1073/pnas.2025030118.
15. Escribá, R.; Larrañaga-Moreira, J.M.; Richaud-Patin, Y.; Pourchet, L.; Lazis, I.; Jiménez-Delgado, S.; Morillas-García, A.; Ortiz-Genga M.; Ochoa, J.P.; Carreras, D.; et al. iPSC-Based Modeling of Variable Clinical Presentation in Hypertrophic Cardiomyopathy. *Circ. Res.* **2023**, *133*, 108–119. https://doi.org/10.1161/CIRCRESAHA.122.321951.
16. Loiben, A.M.; Chien, W.M.; Friedman, C.E.; Chao, L.S.; Weber, G.; Goldstein, A.; Sniadecki, N.J.; Murry, C.E.; Yang, K.C. Cardiomyocyte Apoptosis Is Associated with Contractile Dysfunction in Stem Cell Model of *MYH7* E848G Hypertrophic Cardiomyopathy. *Int. J. Mol. Sci.* **2023**, *24*, 4909. https://doi.org/10.3390/ijms24054909.

© 2025 by the author(s). Distributed under a Creative Commons CC BY license.

Preprints.org (www.preprints.org) | NOT PEER-REVIEWED | Posted: 22 December 2025 doi:10.20944/preprints202512.1808.v1

17. Desai, D.; Song, T.; Singh, R.R.; Baby, A.; McNamara, J.; Green, L.C.; Nabavizadeh, P.; Ericksen, M.; Bazrafshan, S.; Natesan, S.; Sadayappan, S. *MYBPC3* D389V Variant Induces Hypercontractility in Cardiac Organoids. *Cells* **2024**, *13*, 1913. https://doi.org/10.3390/cells13221913.
18. Guo, G.; Wang, L.; Li, X.; Fu, W.; Cao, J.; Zhang, J.; Liu, Y.; Liu, M.; Wang, M.; Zhao, G.; et al. Enhanced myofilament calcium sensitivity aggravates abnormal calcium handling and diastolic dysfunction in patient-specific induced pluripotent stem cell-derived cardiomyocytes with *MYH7* mutation. *Cell Calcium* **2024**, *117*, 102822. https://doi.org/10.1016/j.ceca.2023.102822.
19. Lim, S.; Mangala, M.M.; Holliday, M.; Cserne Szappanos, H.; Barratt-Ross, S.; Li, S.; Thorpe, J.; Liang, W.; Ranpura, G.N.; Vandenberg, J.I.; et al. Reduced connexin-43 expression, slow conduction and repolarisation dispersion in a model of hypertrophic cardiomyopathy. *Dis. Model Mech.* **2024**, *17*, dmm050407. https://doi.org/10.1242/dmm.050407.
20. Mori, H.; Xu, D.; Shimoda, Y.; Yuan, Z.; Murakata, Y.; Xi, B.; Sato, K.; Yamamoto, M.; Tajiri, K.; Ishizu, T.; et al. Metabolic remodeling and calcium handling abnormality in induced pluripotent stem cell-derived cardiomyocytes in dilated phase of hypertrophic cardiomyopathy with MYBPC3 frameshift mutation. *Sci. Rep.* **2024**, 14, 15422. https://doi.org/10.1038/s41598-024-62530-0.
21. Pavlova, S.V.; Shulgina, A.E.; Zakian, S.M.; Dementyeva, E.V. Studying Pathogenetic Contribution of a Variant of Unknown Significance, p.M659I (c.1977G > A) in *MYH7,* to the Development of Hypertrophic Cardiomyopathy Using CRISPR/Cas9-Engineered Isogenic Induced Pluripotent Stem Cells. *Int. J. Mol. Sci.* **2024**, *25*, 8695. https://doi.org/ doi:10.3390/ijms25168695.
22. Steczina, S.; Mohran, S.; Bailey, L.R.J.; McMillen, T.S.; Kooiker, K.B.; Wood, N.B.; Davis, J.; Previs, M.J.; Olivotto, I.; Pioner, J.M.; et al. MYBPC3-c.772G>A mutation results in haploinsufficiency and altered myosin cycling kinetics in a patient induced stem cell derived cardiomyocyte model of hypertrophic cardiomyopathy. *J. Mol. Cell. Cardiol.* **2024**, *191*, 27–39. https://doi.org/10.1016/j.yjmcc.2024.04.010.
23. Beck, M.R.; Dixon, R.D.; Goicoechea, S.M.; Murphy, G.S.; Brungardt, J.G.; Beam, M.T.; Srinath, P.; Patel, J.; Mohiuddin, J.; Otey, C.A.; Campbell, S.L. Structure and function of palladin's actin binding domain. *J. Mol. Biol.* **2013**, *425*, 3325–3337. https://doi.org/10.1016/j.jmb.2013.06.016.
24. Blum, M.; Andreeva, A.; Florentino, L.C.; Chuguransky, S.R.; Grego, T.; Hobbs, E.; Pinto, B.L.; Orr, A.; Paysan-Lafosse, T.; Ponamareva, I.; et al. InterPro: the protein sequence classification resource in 2025. *Nucleic Acids Res.* **2025**, *53*, D444–D456. https://doi.org/10.1093/nar/gkae1082.
25. Jay, J.J.; Brouwer, C. Lollipops in the Clinic: Information Dense Mutation Plots for Precision Medicine. *PLoS One* **2016**, *11*, e0160519. https://doi.org/10.1371/journal.pone.0160519.
26. Okita, K.; Yamakawa, T.; Matsumura, Y.; Sato, Y.; Amano, N.; Watanabe, A.; Goshima, N.; Yamanaka, S. An efficient nonviral method to generate integration-free human-induced pluripotent stem cells from cord blood and peripheral blood cells. *Stem Cells* **2013**, *31*, 458–466. https://doi.org/10.1002/stem.1293.
27. Burridge, P.W.; Matsa, E.; Shukla, P.; Lin, Z.C.; Churko, J.M.; Ebert, A.D.; Lan, F.; Diecke, S.; Huber, B.; Mordwinkin, N.M.; et al. Chemically defined generation of human cardiomyocytes. *Nat. Methods* **2014**, *11*, 855–860. https://doi.org/10.1038/nmeth.2999.
28. Feyen, D.A.M.; McKeithan, W.L.; Bruyneel, A.A.N.; Spiering, S.; Hörmann, L.; Ulmer, B.; Zhang, H.; Briganti, F.; Schweizer, M.; Hegyi, B.; et al. Metabolic Maturation Media Improve Physiological Function of Human iPSC-Derived Cardiomyocytes. *Cell Rep.* **2020**, *32*, 107925. https://doi.org/10.1016/j.celrep.2020.107925.
29. Huby, A.C.; Mendsaikhan, U.; Takagi, K.; Martherus, R.; Wansapura, J.; Gong, N.; Osinska, H.; James, J.F.; Kramer, K.; Saito, K.; et al. Disturbance in Z-disk mechanosensitive proteins induced by a persistent mutant myopalladin causes familial restrictive cardiomyopathy. *J. Am. Coll. Cardiol.* **2014**, 64, 2765–2776. https://doi.org/10.1016/j.jacc.2014.09.071.
30. Refaat, M.M.; Hassanieh, S.; Ballout, J.A.; Zakka, P.; Hotait, M.; Khalil, A.; Bitar, F.; Arabi, M.; Arnaout, S.; Skouri, H.; et al. Non-familial cardiomyopathies in Lebanon: exome sequencing results for five idiopathic cases. *BMC Med. Genomics* **2019**, *12*, 33. https://doi.org/10.1186/s12920-019-0478-7.
31. Chen, Y.; Barajas-Martinez, H.; Zhu, D.; Wang, X.; Chen, C.; Zhuang, R.; Shi, J.; Wu, X.; Tao, Y.; Jin, W. et al. Novel trigenic CACNA1C/DES/MYPN mutations in a family of hypertrophic cardiomyopathy with

© 2025 by the author(s). Distributed under a Creative Commons CC BY license.

Preprints.org (www.preprints.org) | NOT PEER-REVIEWED | Posted: 22 December 2025 doi:10.20944/preprints202512.1808.v1

early repolarization and short QT syndrome. *J. Transl. Med.* **2017**, *15*, 78. https://doi.org/10.1186/s12967-017-1180-1.

32. Hong, M.; Ebana, Y.; Shim, J.; Choi, E.K.; Lim, H.E.; Hwang, I.; Yu, H.T.; Kim, T.H.; Uhm, J.S.; Joung, B. et al. Ethnic similarities in genetic polymorphisms associated with atrial fibrillation: Far East Asian vs European populations. *Eur. J. Clin. Invest.* **2021**, *51*, e13584. https://doi.org/10.1111/eci.13584.
33. Meng, X.; Nie, Y.; Wang, K.; Fan, C.; Zhao, J.; Yuan, Y. Identification of Atrial Fibrillation-Associated Genes ERBB2 and MYPN Using Genome-Wide Association and Transcriptome Expression Profile Data on Left-Right Atrial Appendages. *Front. Genet.* **2021**, *12*, 696591. https://doi.org/10.3389/fgene.2021.696591.
34. Ma, K.; Wang, K. Interaction of nebulin SH3 domain with titin PEVK and myopalladin: implications for the signaling and assembly role of titin and nebulin. *FEBS Lett.* **2002**, *532*, 273–278. https://doi.org/10.1016/s0014-5793(02)03655-4.
35. Gu, Q.; Mendsaikhan, U.; Khuchua, Z.; Jones, B.C.; Lu, L.; Towbin, J.A.; Xu, B.; Purevjav, E. Dissection of Z-disc myopalladin gene network involved in the development of restrictive cardiomyopathy using system genetics approach. *World J. Cardiol.* **2017**, *9*, 320–331. https://doi.org/10.4330/wjc.v9.i4.320.
36. Kojic, S.; Medeot, E.; Guccione, E.; Krmac, H.; Zara, I.; Martinelli, V.; Valle, G.; Faulkner, G. The Ankrd2 protein, a link between the sarcomere and the nucleus in skeletal muscle. *J. Mol. Biol.* **2004**, *339*, 313–325. https://doi.org/10.1016/j.jmb.2004.03.071.
37. Klimenko, E.S.; Sukhareva, K.S.; Vlasova, Y.; Smolina, N.A.; Fomicheva, Y.; Knyazeva, A.; Muravyev, A.S.; Sorokina, M.Y.; Gavrilova, L.S.; Boldyreva, L.V.; et al. Flnc expression impacts mitochondrial function, autophagy, and calcium handling in C2C12 cells. *Exp. Cell Res.* **2024**, *442*, 114174. https://doi.org/10.1016/j.yexcr.2024.114174.
38. Klimenko, E.S.; Zaytseva, A.K.; Sorokina, M.Yu.; Perepelina, K.I.; Rodina, N.L.; Nikitina, E.G.; Sukhareva, K.S.; Khudiakov, A.A.; Vershinina, T.L.; Muravyev, A.S.; et al. Distinct molecular features of *FLNC* mutations, associated with different clinical phenotypes. Cytoskeleton **2025**, *82*, 158-174. https://doi.org/10.1002/cm.21922.
39. Altschul, S.F.; Gish, W.; Miller, W.; Myers, E.W.; Lipman, D.J. Basic local alignment search tool. *J. Mol. Biol.* **1990**, *215*, 403–410. https://doi.org/10.1016/S0022-2836(05)80360-2.
40. Sievers, F.; Wilm, A.; Dineen, D.; Gibson, T.J.; Karplus, K.; Li, W.; Lopez, R.; McWilliam, H.; Remmert, M.; Söding, J.; et al. Fast, scalable generation of high-quality protein multiple sequence alignments using Clustal Omega. *Mol. Syst. Biol.* **2011**, *7*, 539. https://doi.org/10.1038/msb.2011.75.
41. Waterhouse, A.M.; Procter, J.B.; Martin, D.M.A.; Clamp, M.; Barton, G.J. Jalview Version 2—a multiple sequence alignment editor and analysis workbench. *Bioinformatics* **2009**, *25*, 1189–1191. https://doi.org/10.1093/bioinformatics/btp033.
42. Berman, H.M.; Westbrook, J.; Feng, Z.; Gilliland, G.; Bhat, T.N.; Weissig, H.; Shindyalov, I.N.; Bourne, P.E. The Protein Data Bank. *Nucleic Acids Res.* **2000**, *28*, 235–242. https://doi.org/10.1093/nar/28.1.235.
43. Wang, X.F.; Chen, Z.; Wang, C.; Yan, R.X.; Zhang, Z.; Song, J. Predicting residue-residue contacts and helix-helix interactions in transmembrane proteins using an integrative feature-based random forest approach. *PLoS One* **2011**, *6*, e26767. https://doi.org/10.1371/journal.pone.0026767.
44. Liu, X.; Li, C.; Mou, C.; Dong, Y.; Tu, Y. dbNSFP v4: a comprehensive database of transcript-specific functional predictions and annotations for human nonsynonymous and splice-site SNVs. *Genome Med.* **2020**, *12*, 103. https://doi.org/10.1186/s13073-020-00803-9.
45. Sorogina, D.A.; Grigor'eva, E.V.; Malakhova, A.A.; Pavlova, S.V.; Medvedev, S.P.; Vyatkin, Y.V.; Khabarova, E.A.; Rzaev, J.A.; Zakian, S.M. Creation of Induced Pluripotent Stem Cells ICGi044-B and ICGi044-C Using Reprogramming of Peripheral Blood Mononuclear Cells of a Patient with Parkinson's Disease Associated with c.1492T>G Mutation in the *GLUD2* Gene. *Russ. J. Dev. Biol.* **2023**, *54*, 104–111. https://doi.org/10.1134/S1062360423010125.
46. Khudiakov, A.; Zaytseva, A.; Perepelina, K.; Smolina, N.; Pervunina, T.; Vasichkina, E.; Karpushev, A.; Tomilin, A.; Malashicheva, A.; Kostareva, A. Sodium current abnormalities and deregulation of Wnt/β-catenin signaling in iPSC-derived cardiomyocytes generated from patient with arrhythmogenic cardiomyopathy harboring compound genetic variants in plakophilin 2 gene. *Biochim. Biophys. Acta Mol. Basis Dis.* **2020**, *1866*, 165915. https://doi.org/10.1016/j.bbadis.2020.165915.

© 2025 by the author(s). Distributed under a Creative Commons CC BY license.

Preprints.org (www.preprints.org) | NOT PEER-REVIEWED | Posted: 22 December 2025 doi:10.20944/preprints202512.1808.v1

Disclaimer/Publisher's Note: The statements, opinions and data contained in all publications are solely those of the individual author(s) and contributor(s) and not of MDPI and/or the editor(s). MDPI and/or the editor(s) disclaim responsibility for any injury to people or property resulting from any ideas, methods, instructions or products referred to in the content.

© 2025 by the author(s). Distributed under a Creative Commons CC BY license.